مجلة الدراسات التربوية والعلمية - كلية التربية - الجامعة العراقية
العدد السادس والعشرون - المجلد الأول - علوم الفيزياء - أيلول 2025 م
doi.org/10.52866/esj.2025.01.26.23

# Calculation of nuclear radii and deformation parameters for isotopes of selenium and krypton nuclei

**Reem gani abdulrazzaq mohammeda , Sameera Ahmed Ebrahiem**
a,b Department of Physics, College of Education for pure science Ibn Al-Haitham, University of Baghdad
aReem.Mohammed1704d@ihcoedu.uobaghdad.edu.iq , b sameera.a.i@ihcoedu.uobaghdad.edu.iq

**Abstract**:
This study included the calculation of the distortion coefficient derived from the electric quadrupole moments Qo and the distortion coefficients , which arise from low electrical transition potential (B (E2)↑ in e2 b2 unit, based on the excitation energy +2 specifically for the even-even nuclei of the element Selenium-34 and for mass numbers between 70-84. Since the distortion parameter β2 is a model based on quantum mechanics, Consider that it describes the interaction of a nucleon Along with all the other nucleons in the nucleus, it can be calculated from the low electrical transition potential (B (E2)↑ in e2 b2 unit, which depends on the gamma energy, which is measured in units the KeV and the mass number. In general, the shape of the nucleus is spherical when the nucleus is stable, as this voltage reduces the surface energy of the nucleus, as shown in the declared values for nucleons with magic numbers .The root mean square of the radius was calculated and compared with previous studies, and the major and minor axes (b, a) were calculated.. The values of ΔR were calculated, which indicates the deviation between the minor semi-axis b and the major semi-axis a is included in the calculation of the delta distortion coefficient.

**Key word**: nuclei , shell model , quadrupole moments , possibility of electrical transition, excitation energy , half-life mean-squared, charge distribution, radius <r2 >.

# حساب اقطار النواة ومعاملات التشوه لنظائر نواة السيلينيوم والكريبتون

**ريم غني عبد الرزاق ، سميره احمد ابراهيم**
قسم الفيزياء، كلية التربية للعلوم الصرفة - ابن الهيثم ، جامعة بغداد، بغداد، العراق

**مستخلص:**
تضمنت هذه الدراسة حساب معامل التشوه المشتق من عزم الرباعي الكهربائي $Q_0$ ومعاملات التشوه، والتي تنشأ من جهد انتقال كهربائي منخفض ↑ (B (E2) في وحدة $e^2\ b^2$ ، بناءً على طاقة الإثارة +2 خصيصًا للنوى الزوجية الزوجية لعنصر السيلينيوم ولأعداد الكتلة بين 70-84 . نظرًا لأن معامل التشوه β2 هو نموذج يعتمد على ميكانيكا الكم، فضع في اعتبارك أنه يصف تفاعل النيوكليون مع جميع النيوكليونات الأخرى في النواة، ويمكن حسابه من جهد الانتقال الكهربائي المنخفض ↑ (B (E2) في وحدة $e^2\ b^2$ ، والذي يعتمد على طاقة جاما، والتي تقاس بوحدات KeV والعدد الكتلي. بشكل عام، يكون شكل النواة كرويًا عندما تكون النواة مستقرة، حيث يقلل هذا الجهد من طاقة سطح النواة، كما هو موضح في القيم المعلنة للنيوكليونات ذات الأرقام السحرية. جذر متوسط مربع تم حساب نصف القطر ومقارنته مع الدراسات السابقة، وتم حساب المحورين الرئيسي والثانوي (ب، أ). وتم حساب قيم ΔR التي تشير إلى أن الانحراف بين نصف المحور الثانوي (ب) وشبه المحور الرئيسي (أ) يدخل في حساب معامل تشوه δ .

**الكلمات المفتاحية**: عزم رباعي القطب، إمكانية الانتقال الكهربائي، متوسط عمر النصف التربيعي، توزيع الشحنة، نصف القطر <r2>.

## Introduction

In this model, different parts of the nucleus move independently, contrasting with the liquid drop model, which describes the nucleus as an incompressible fluid where the motion of one part influences all adjacent regions. Another perspective on nuclear structure is provided by the collective model, which integrates aspects of both the shell model and the liquid drop model.

The liquid drop model assumes that all nuclei have similar mass densities, analogous to a charged liquid droplet, where nuclear energies are approximately proportional to mass. A key result of this model is the Semi-Empirical Mass Formula (SEMF), which effectively explains binding energies and average nuclear masses. Meanwhile, the shell model, grounded in quantum mechanics, solves the Schrödinger equation[1] to describe the nucleus as a spherical system. Although it shares fundamental assumptions with the Fermi gas model, the shell model incorporates a significant spin- orbit interaction. This allows it to accurately predict nuclear properties such as ground-state spin, parity, magic numbers, and the SEMF coupling term.

The collective model, also based on quantum mechanics, extends these predictions to include electric and magnetic dipole moments. However, unlike the shell model, it allows for distortions in the nuclear shape depending on the potential involved.

In even-mass nuclei, configurations with even or odd numbers of protons (Z) and neutrons (N) are possible. However, as will be discussed later, only a limited number of odd-odd nuclei exist, and all stable nuclei in this category tend to have an even number of protons or neutrons[2]

**Theory :**

Nuclear deformation arises from the arrangement of valence nucleons within the unfilled nuclear shells. Distortion occurs only when both proton (P) and neutron (n) shells are not completely filled[3]. One fundamental type of nuclear deformation is quadrupole distortion, where the nucleus may adopt either a prolate (elongated) or oblate (flattened) shape, as illustrated in the accompanying figure1 [4].

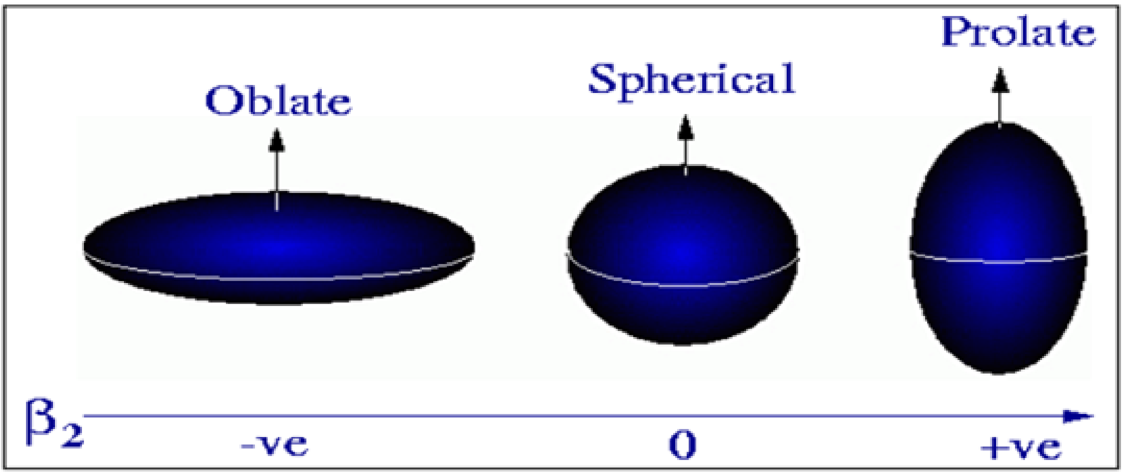


Figure .1. A diagram with flattened, stretched shapes and spherical. Arrows on the flattened and stretched shapes indicate symmetry [5].

their liquid drop model of the nucleus supple and soft, thus permitting them to detect considerable distortions in its shape from a perfect sphere. Anywhere the number of neutron (N) had a high frequency, a considerable number of nuclei were identified (N) and protons (P) is markedly distant from the magnetic values, exhibiting a distorted charge distribution[6].

The distortion parameter β2 is a model based on quantum mechanics [7]. Considering that these probabilities describe the interactions of nucleons with all other nucleons in all remainder nucleons in the nucleus [8]:

$$\beta_2 = 4\pi / 3ZR_o^2 \, [\, B(E2)\uparrow e^2 b^2 / e^2 \,]^{1/2} \quad \text{.............(1)}$$

$$\text{Where} \quad R_o = 0.0144\, A^{1/3} \quad \text{..............(2)}$$

$$\text{And} \quad B(E2)\uparrow = 2.6\, E\gamma^{-1} Z^2 A^{-2/3} \quad \text{...................(3)}$$

In this context, A denotes the mass number of a nucleus, Z represents the atomic number, and $E\gamma$ signifies the gamma-ray transitions energy, measured in kiloelectronvolts (KeV).

To calculate the deformation parameter δ, we rely on the internal electric quadrupole $Q_o$ because it provides information on deformation and shape, measuring the distortion and spherical symmetry of the charge distribution. [9]. The quadrilateral deformation coefficient (the degree of variation in the spherical shape) can be calculated using the quadrilateral moments $Q_o$ [10].

$$\delta = 0.75 Q_o / (< r^2 > Z) \quad \text{................(4)}$$

Where $Q_o = [(16\pi/5)\, B(E2) e^2 b^2 / e^2]^{1/2}$ ...............(5)

The average radius $< r2 >$ can be calculated:

$$< r^2 > = 0.63 R_o^2 (1+10/3(\pi a_o/R_o)^2)/(1+(\pi a_o/R_o)^2)\ (A \leq 100) \quad \text{.............(6)}$$

Whence the Ro: radial Woods-Saxon parameters are, Ro=1.07A1/3 fm and ao=0.55(fm), with ao from fast electron scattering information [11].

In general, shapes of nuclei are approximately spherical when a nucleus is stable[12], since it lowers the surface energy of the nucleus [13]. Hence, small sections of spheres are seen, as with the region 150<A<190

$$\delta = \Delta R / R \quad \text{.......................(7)}$$

Where:

ΔR denotes the difference between the semi-major and semi-minor axes[14].

While the average of the nuclear radius represents by R, due to, as assumed,

$$\Delta R = (b - a) \quad \text{.................(8)}$$

The subsequent equations provide the semi-axes (a) and (b) [2].

$$a = \sqrt{< r2 > (1.66 - \frac{2\delta}{0.9})} \quad \text{........ (9)}$$

$$b = \sqrt{5 < r2 > - 2a^2} \quad \text{......(10)}$$

## Result:

The research deals with the analysis of the nuclear properties of even-even isotopes of selenium and krypton, by comparing the experimental and theoretical values of the nuclear deformation factors, the probability of the electrical transition B(E2) $B(E2; 0_1^+ \rightarrow 2_1^+)$ [15] , and the quadrupole moment $Q_o$. In selenium isotopes, we note in Table (1) that the nuclear deformation factor [16]gradually decreases with increasing mass number, reaching a value of 0.1452 at the isotope A=84 (magic number of neutrons), where the nucleus becomes more stable and spherical[17]. We note that the quadrupole moment $Q_o$ gradually increases, reflecting the increase in nuclear deformation with increasing mass number[18]. In the probability of the electrical transition B(E2), it increases with the mass number until it reaches a maximum value, then begins to gradually decrease.

As for Table (2), the gamma energy starts at 709 eV at A=72, decreases until A=82 (magic number) and then rises again[3].

Table (3) shows a good agreement between the theoretical and experimental values of the nuclear radius[19] and the semi-major and minor axes, indicating a gradual expansion in the nuclear volume.

As for the krypton isotopes in Table (4), the distortion parameters show a slight increase with increasing mass number, then tend to stabilize after reaching certain isotopes. The distortion coefficient delta gradually decreases, indicating that the shape of the nucleus is converging towards the spherical. In the probability of electrical transition B(E2), it increases with the mass number until it reaches a maximum value, then begins to decrease as shown in Figure (5). It was shown that the quadrupole moment Qo increases gradually, then stabilizes relatively with heavier isotopes, reflecting the stability of the electrical charge distribution.

In Table (5), the gamma energy [20] starts at 709 eV at A=72, decreases until A=82, then returns to increase.

As for Table (6), it was shown that the average nuclear radius[19] shows agreement between the experimental and theoretical values, indicating the stability of the nuclear shape.

## Conclusions:

Analysis of the results of the previous data and the observed results for the given stationary nuclei shows that the energy of the first state 2+ varies smoothly with A. It has been observed that the nucleons fall outside the conditions of partial or complete oscillation which polarize in one direction and thus lead to permanent deformation of the nucleus. Consequently, these nuclei will take stable non-spherical shapes. The results indicate that the nuclear deformation in both elements gradually decreases with increasing mass number, with relative stability in the heavier isotopes. The motion of the nucleons will be just outside the closed shell; as they approach the magic number, they are particularly stable and increase in rotational motion as well as deformation of the nucleus.

**Table 1. Quadripole moment Tetrapolar electrode ($Q_o$) in barns, gamma energy to the first level Eγ, low electrostatic transition potential B(E2)↑ in $e^2$ $b^2$ units, average nuclear radius ($Ro^2$), number of neutrons (N), mass numbers of isotopes (A) Iron and parameters of deformation (β2, δ) for selenium Se.**

| Z | A | N | The Theoretical Values | | A presnt Work | | | | | |
|---|---|---|---|---|---|---|---|---|---|---|
| | | | $E_\gamma(keV)$ | B(E)↑ ($e^2b^2$) for Global Best Fit | $\beta_2$ for Global Best Fit | $\delta$ | $\beta_2$ | $Q_o$ | B(E2)↑ e2b2 | $R_o2$ |
| 34 | 70 | 36 | 944.6 | 0.185 | 0.2167 | 0.1574 | 0.2180 | 1.3723 | 0.1873 | 24.46 |
| | 72 | 38 | 862.08 | 0.199 | 0.2205 | 0.1608 | 0.2219 | 1.4231 | 0.2014 | 24.92 |
| | 74 | 40 | 634.75 | 0.265 | 0.2499 | 0.1830 | 0.2516 | 1.6434 | 0.2686 | 25.38 |
| | 76 | 42 | 559.101 | 0.30 | 0.2612 | 0.1905 | 0.2610 | 1.7355 | 0.2996 | 25.84 |
| | 78 | 44 | 613.725 | 0.265 | 0.2413 | 0.1778 | 0.2427 | 1.6422 | 0.2683 | 26.29 |
| | 80 | 46 | 666.16 | 0.240 | 0.2257 | 0.1670 | 0.2272 | 1.5630 | 0.2430 | 26.74 |
| | 84 | 50 | 1454.42 | 0.106 | 0.1452 | 0.1083 | 0.1464 | 1.0407 | 0.1077 | 27.62 |

**Table 2. Average half-life t (s) for iron (Fe) isotopes, neutron numbers N, gamma energy to the first state, probability T of transition, and A represent mass numbers.**

| Z | A | N | $E_i(keV)$ | $E_\gamma(keV)$ | $t_{1/2}$ (s) | T (s) | $\tau$ (s) |
|---|---|---|---|---|---|---|---|
| 34 | 70 | 36 | 994 | 994.6 | 1.0ps*$10^{-12}$ | $10^{-12}$*1.4430 | $10^{11}$*6.9300 |
| | 72 | 38 | 862 | 862.08 | ps$10^{-12}$*3.0 | $10^{-12}$*4.3290 | $10^{11}$*2.3100 |
| | 74 | 40 | 634 | 634.75 | 7.08ps*$10^{-12}$ | $10^{-11}$*1.0216 | $10^{10}$*9.7881 |
| | 76 | 42 | 559 | 559.101 | 12.3ps*$10^{-12}$ | $10^{-11}$*1.7749 | $10^{10}$*5.6341 |
| | 78 | 44 | 613 | 613.727 | 9.7ps*$10^{-12}$ | $10^{-11}$*1.3997 | $10^{10}$*7.1443 |
| | 80 | 46 | 666 | 666.16 | 8.56ps*$10^{-12}$ | $10^{-11}$*1.2352 | $10^{10}$*8.0958 |
| | 84 | 50 | 1454 | 1454.42 | (3.10m)186 | 268.3983 | 0.0037 |

**Table 3. Additionally, it includes the mass numbers (A), the major and minor axes (b, a), neutron counts (N), the root mean square of the radius $<r^2>^{(1/2)}$, as well as their separation (ΔR) for the isotopes of iron, described in two distinct ways.**

| Z | A | N | A Theortical value | Present work | | | | | | |
|---|---|---|---|---|---|---|---|---|---|---|
| | | | $<r_2>_{1/2}$ [21] | $<r^2>$ (fm) | $<r^2>^{1/2}$ (fm) | a (fm) | b (fm) | $\Delta R_1$ | $\Delta R_2$ | $\Delta R_3$ |
| 34 | 70 | 36 | ………… | 19.2325 | 4.3854 | 2.4032 | 3.2213 | 0.6941 | 0.8182 | 1.0202 |
| | 72 | 38 | ………… | 19.5220 | 4.4183 | 2.4052 | 3.2437 | 0.7158 | 0.8385 | 1.0480 |
| | 74 | 40 | 4.0700 | 19.8085 | 4.4506 | 2.3681 | 3.3223 | 0.8221 | 0.9542 | 1.1992 |
| | 76 | 42 | 4.1395 | 20.0921 | 4.4824 | 2.3607 | 3.3566 | 0.8636 | 0.9959 | 1.2553 |
| | 78 | 44 | 4.1406 | 20.3729 | 4.5136 | 2.3957 | 3.3301 | 0.8129 | 0.9345 | 1.1776 |
| | 80 | 46 | 4.1400 | 20.6510 | 4.5443 | 2.4265 | 3.3085 | 0.7698 | 0.8820 | 1.1113 |
| | 84 | 48 | …………. | 21.1996 | 4.6043 | 2.5624 | 3.1448 | 0.5075 | 0.5824 | 0.7281 |

**Table 4. Quadripole moment Tetrapolar electrode ($Q_o$) in barns, gamma energy to the first level $E^{\gamma}$, low electrostatic transition potential B(E2)↑ in $e^2$ $b^2$ units, average nuclear radius ($Ro^2$), number of neutrons (N), mass numbers of isotopes (A) Iron and parameters of deformation (β2, δ) for krypton.**

| Z | A | N | E_γ (keV) | The Theoretical Values | | A present Work | | | | |
|---|---|---|---|---|---|---|---|---|---|---|
| | | | | $B(E_2)\uparrow(e^2b^2)$ for Global Best Fit | $\beta_2$ for Global Best Fit | $\delta$ | $\beta_2$ | Q∘ (b) | $B(E_2)\uparrow(e^2b^2)$ | $R_\circ^2$ |
| 36 | 72 | 36 | 709.1 | 0.271 | 0.2430 | 0.1773 | 0.2447 | 1.6615 | 0.2746 | 24.92 |
| | 74 | 38 | 455.80 | 0.91 | 0.2935 | 0.2160 | 0.2969 | 2.0302 | 0.4194 | 25.38 |
| | 76 | 40 | 423.96 | 0.44 | 0.2987 | 0.2188 | 0.2997 | 2.1103 | 0.4430 | 25.84 |
| | 78 | 42 | 455.04 | 0.40 | 0.2799 | 0.2065 | 0.2819 | 2.0194 | 0.4056 | 26.29 |
| | 80 | 44 | 616.61 | 0.29 | 0.2344 | 0.1735 | 0.2361 | 1.7202 | 0.2943 | 0.2674 |
| | 82 | 46 | 776.521 | 0.227 | 0.2040 | 0.1514 | 0.2053 | 1.5203 | 0.2299 | 27.18 |
| | 84 | 48 | 881.615 | 0.197 | 0.1870 | 0.1391 | 0.1881 | 1.4159 | 0.1994 | 27.62 |
| | 86 | 50 | 1564.87 | 0.109 | 0.1369 | 0.1023 | 0.1379 | 1.0541 | 0.1105 | 28.06 |
| | 88 | 52 | 775.31 | 0.217 | 0.1903 | 0.1424 | 0.1914 | 1.4861 | 0.2197 | 28.49 |
| | 90 | 54 | 707.13 | 0.234 | 0.1946 | 0.1462 | 0.1960 | 1.5445 | 0.2373 | 28.92 |
| | 92 | 56 | 769 | 0.212 | 0.1826 | 0.1375 | 0.1838 | 1.4702 | 0.2150 | 29.35 |
| | 94 | 58 | 665 | 0.242 | 0.1923 | 0.1451 | 0.1935 | 1.5697 | 0.2451 | 29.77 |

**Table 5. Average half-life t (s) for iron (Fe) isotopes, neutron numbers N, gamma energy to the first state, probability T of transition, and A represent mass numbers.**

| Z | A | N | $E_i\,(keV)$ | $E_2\,(keV)$ | $t_{\frac{t}{2}}(s)$ | T(s) | τ(s) |
|---|---|---|---|---|---|---|---|
| 36 | 72 | 36 | 709.1 | 709 | 17.2s | 24.8196 | 0.0403 |
| | 74 | 38 | 455.80 | 455 | (11.50m)690 | 995.6710 | 0.0010 |
| | 76 | 40 | 423.96 | 423 | (14.8h)53.280 | 76.8831 | 0.0130 |
| | 78 | 42 | 455.04 | 455 | (23.9ps)$23.9*10^{-12}$ | $3.4488*10^{-11}$ | $2.8996*10^{10}$ |
| | 80 | 44 | 616.61 | 616 | (8.7ps)$8.7*10^{-12}$ | $1.2554*10^{-11}$ | $7.9655*10^{10}$ |
| | 82 | 46 | 776.521 | 776 | (4.45ps)$4.45*10^{-12}$ | $6.4214*10^{-12}$ | $1.5573*10^{11}$ |
| | 84 | 48 | 881.615 | 881 | (4.35ps)$4.35*10^{-12}$ | $6.2771*10^{-12}$ | $1.5931*10^{11}$ |
| | 86 | 50 | 1564.87 | 1564 | (0.222ps)$0.222*10^{-12}$ | $3.2035*10^{-13}$ | $3.1216*10^{12}$ |
| | 88 | 52 | 775.31 | 775 | (2.84h)10.224 | 14.7532 | 0.0678 |
| | 90 | 54 | 707.13 | 707 | 32.32s | 46.6378 | 0.0214 |
| | 92 | 56 | 769 | 769 | 1.840s | 2.6551 | 0.03766 |
| | 94 | 58 | 665 | 665 | 0.20s | 0.2886 | 3.4650 |

**Table 6. Additionally, it includes the mass numbers (A), the major and minor axes (b, a), neutron counts (N), the root mean square of the radius $<r^2>^{(1/2)}$, as well as their separation (ΔR) for the isotopes of iron, described in two distinct ways.**

| Z | A | N | A Theoretical Values | A present Work | | | | | | |
|---|---|---|---|---|---|---|---|---|---|---|
| | | | $\langle r^2\rangle^{\frac{1}{2}}$ fm | $\langle r^2\rangle\ fm$ | $\langle r^2\rangle^{\frac{1}{2}}$ fm | $a\ (fm)$ | b (fm) | $\Delta R_1$ | $\Delta R_2$ | $\Delta R_3$ |
| 36 | 72 | 36 | 4.1635 | 19.5220 | 4.4183 | 2.3713 | 3.2933 | 0.7892 | 0.9220 | 1.1556 |
| | 74 | 38 | 4.1870 | 19.8085 | 4.4506 | 2.2982 | 3.4190 | 0.9702 | 1.1208 | 1.4152 |
| | 76 | 40 | 4.2020 | 20.0921 | 4.4824 | 2.3002 | 3.4395 | 0.9917 | 1.1392 | 1.4415 |
| | 78 | 42 | 4.2038 | 20.3729 | 4.5136 | 2.3348 | 3.4154 | 0.9441 | 1.0806 | 1.3676 |
| | 80 | 44 | 4.1970 | 20.6510 | 4.5443 | 2.4128 | 3.3285 | 0.8001 | 0.9157 | 1.1551 |
| | 82 | 46 | 4.1919 | 20.9266 | 4.5745 | 2.4669 | 3.2713 | 0.7036 | 0.8044 | 1.0125 |
| | 84 | 48 | 4.1884 | 21.1996 | 4.6043 | 2.5000 | 3.2436 | 0.6520 | 0.7436 | 0.9355 |
| | 86 | 50 | 4.1835 | 21.4702 | 4.6335 | 2.5825 | 3.1351 | 0.4831 | 0.5526 | 0.6910 |
| | 88 | 52 | 4.2171 | 21.7386 | 4.6624 | 2.5090 | 3.2744 | 0.6778 | 0.7654 | 0.9667 |
| | 90 | 54 | 4.2423 | 22.0047 | 4.6909 | 2.5088 | 3.2965 | 0.7012 | 0.7877 | 0.9972 |
| | 92 | 56 | 4.2724 | 22.2686 | 4.7189 | 2.5343 | 3.2787 | 0.6644 | 0.7444 | 0.9423 |
| | 94 | 58 | 4.3002 | 22.5304 | 4.7466 | 2.5259 | 3.3126 | 0.7062 | 0.7867 | 0.9989 |

Figure 2 shows the relationship between the mass number of the element Se and the distortion coefficient delta.

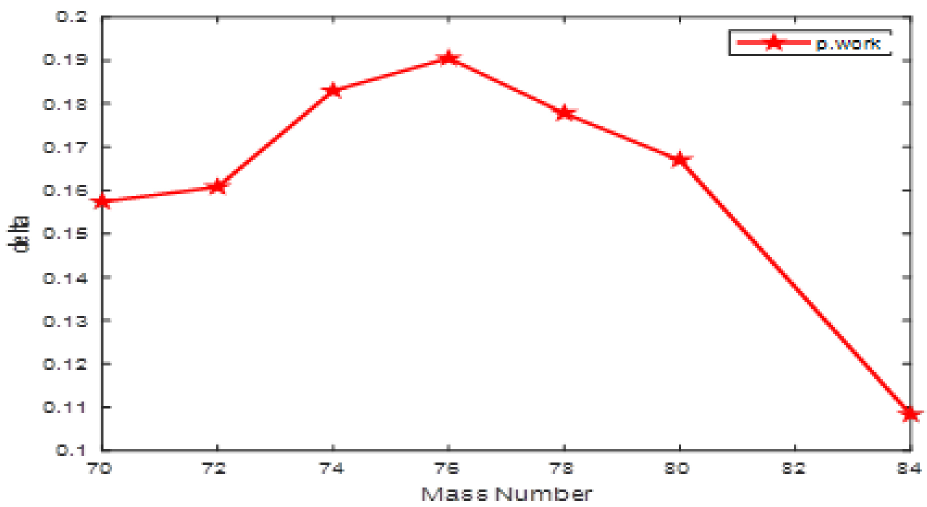


Figure 3 shows the relationship between the mass number of the element Se and the beta distortion factor.

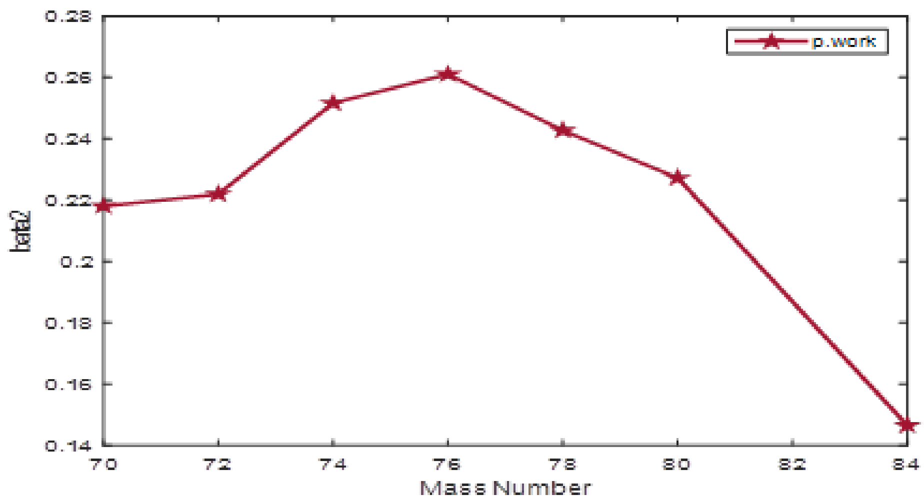


Figure 4 shows the relationship between the mass number of the element Se and the electric quadrupole moment.

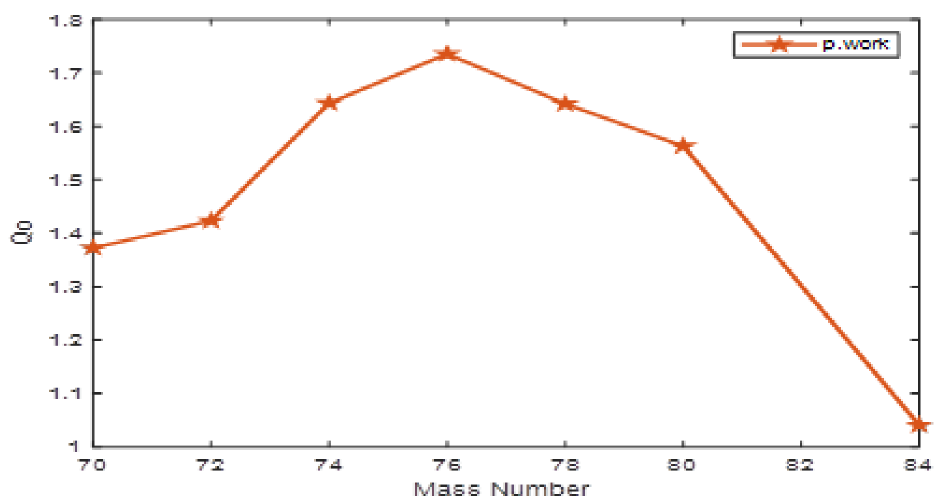

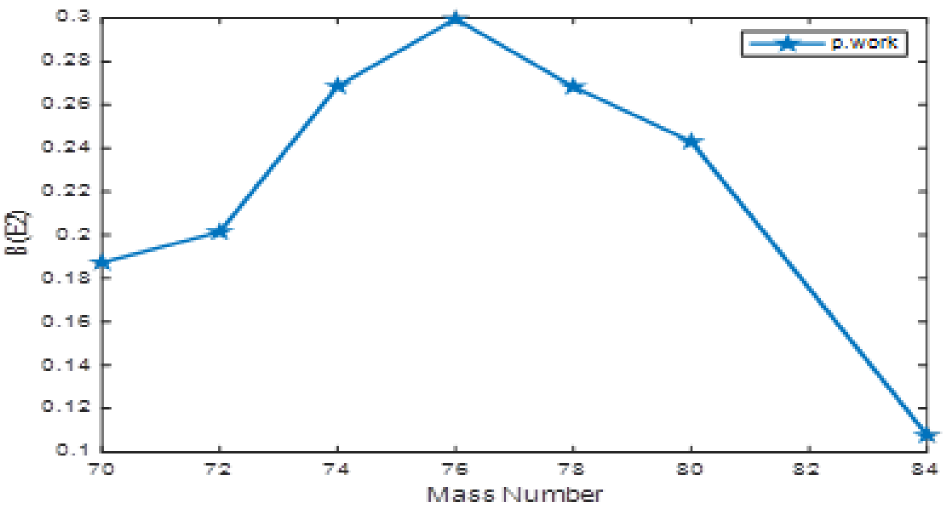


Figure 5 shows the relationship between the mass number of the element Se and the probability of the central quadrupole transition.

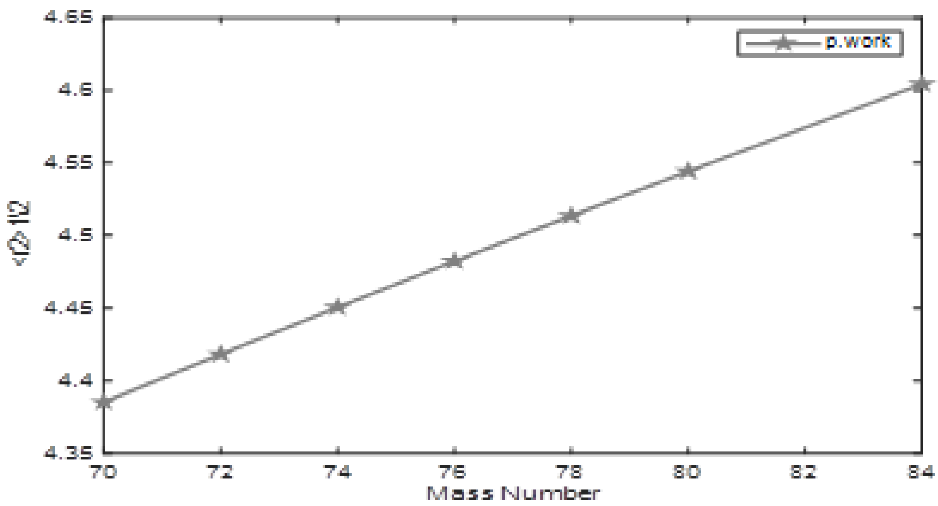


Figure 6 shows the relationship between the mass number of the element Se and the root mean square of the charge radius.

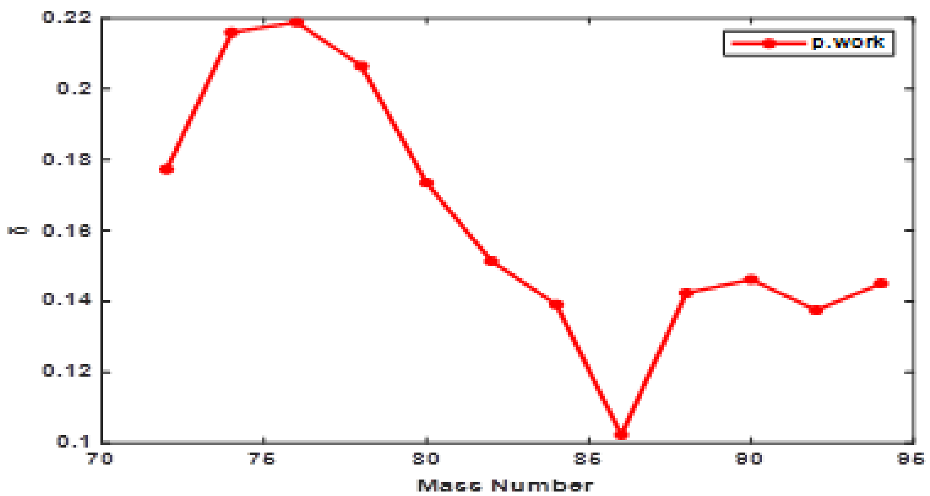


Figure 7 shows the relationship between the mass number of the element Kr and the distortion coefficient delta.

Figure 8 shows the relationship between the mass number of the element Se and the beta distortion factor.

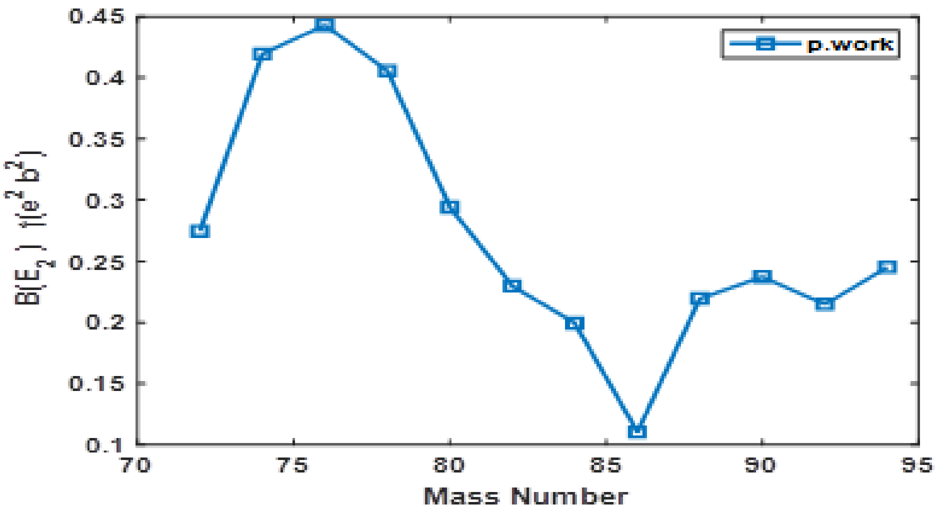


Figure 9 shows the relationship between the mass number of the element Se and the electric quadrupole moment.

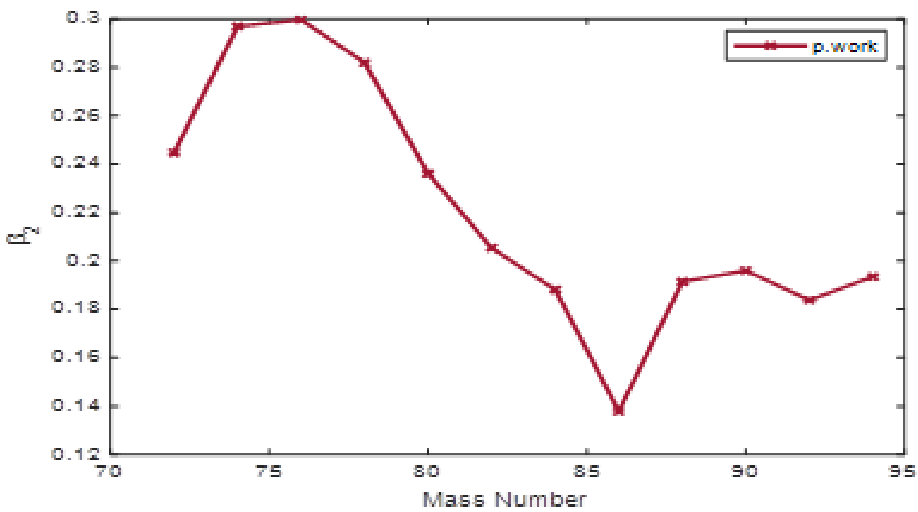


Figure 10 shows the relationship between the mass number of the element Se and the probability of the central quadrupole transition.

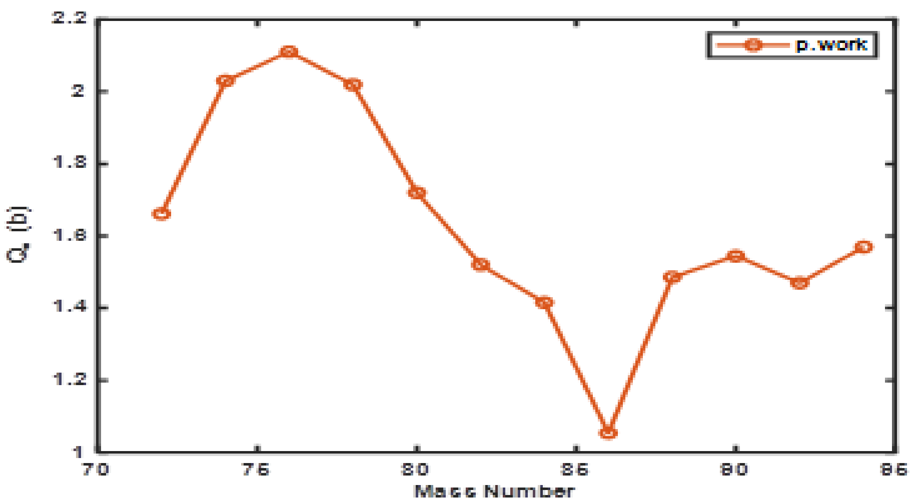

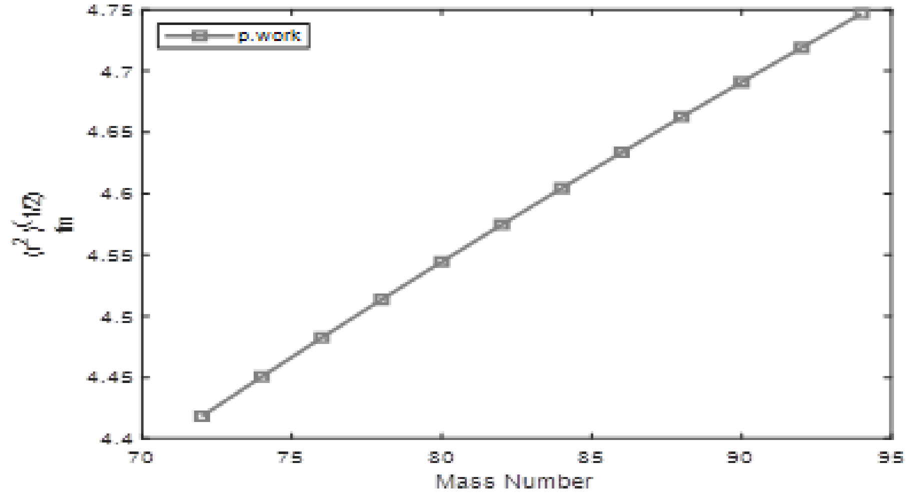


**Figure 11 shows the relationship between the mass number of the element Se and the root mean square of the charge radius.**

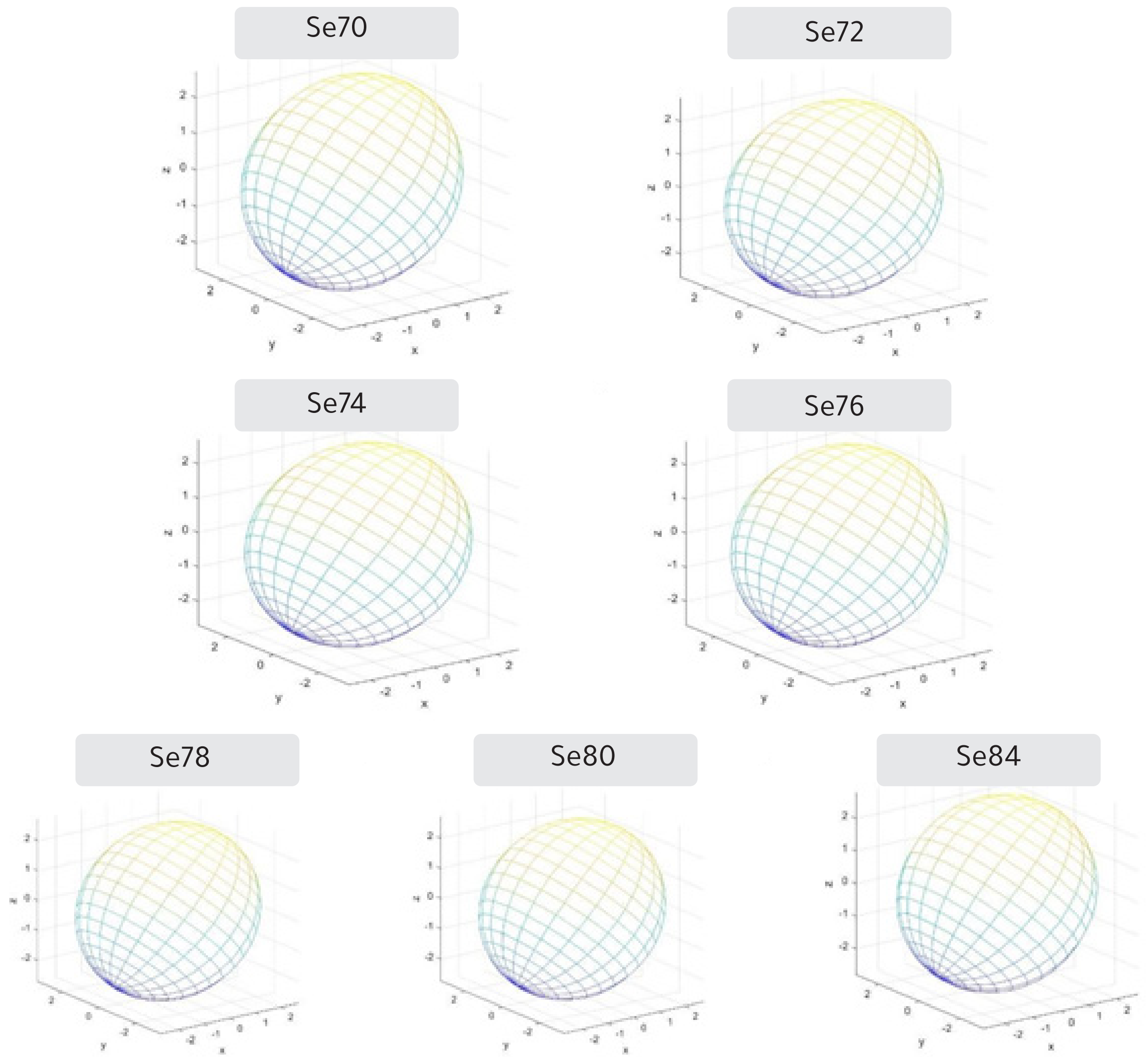


**Figure 12 Three-dimensional shapes of the axially symmetric tetragon, deformation of the selenium $_{34}$Se isotope along the major (a) and minor (b) axis.**

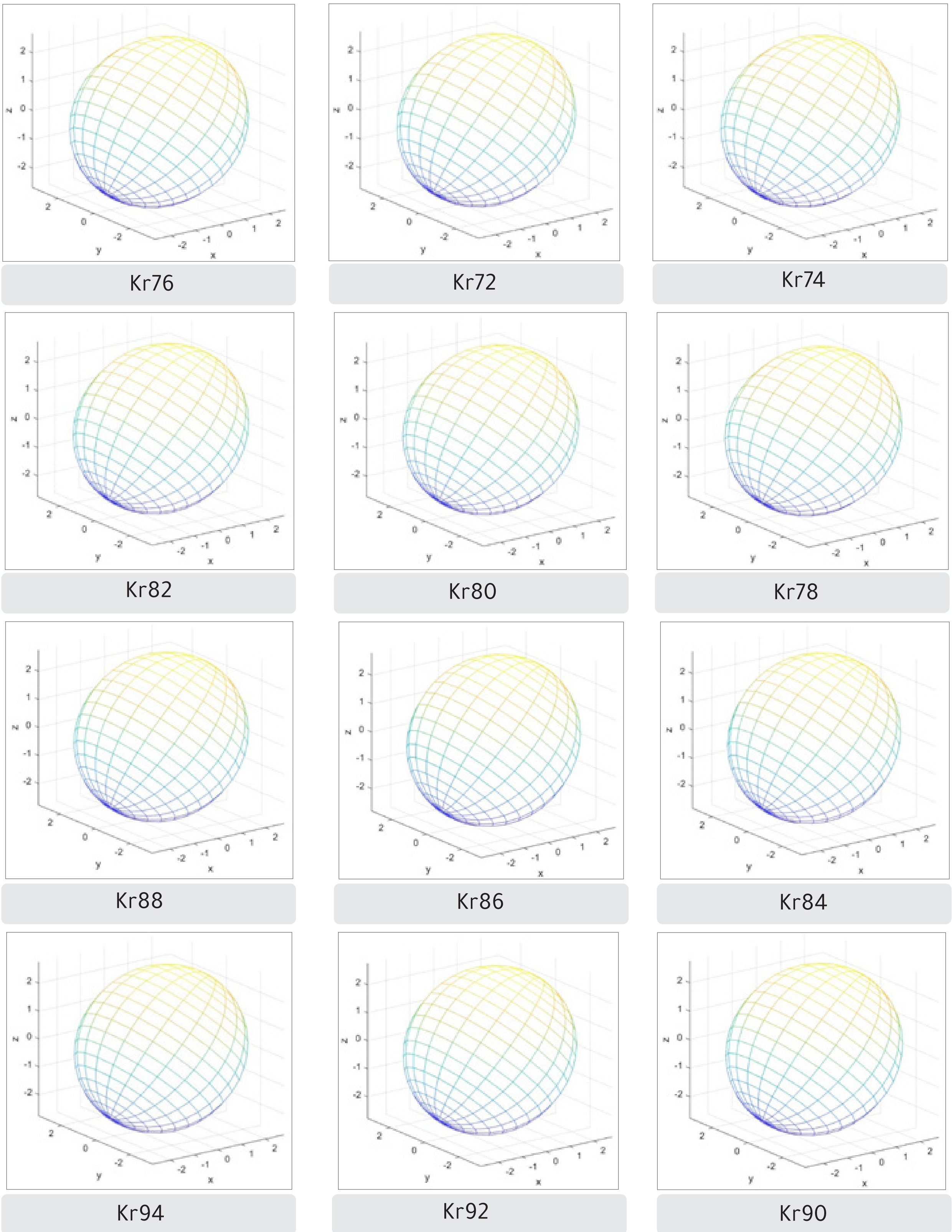


**Figure 13 Three-dimensional shapes of the axially symmetric tetragon, deformation of the kerypton $_{36}$Kr isotope along the major (a) and minor (b) axis.**

## Reference ;


[1] Mohammed NA, Ebrahiem SA. Radioactivity levels of 238U, 234Th, 40K and 137C in the soil surface of selected regions from Baghdad governorate. International Journal of Nuclear Energy Science and Technology 2020;14:15–27.

[2] Ebrahiem SA, AL-khalidi SH. Interaction Samarium and Holmium with Charged ed Particles (Alpha particles). مجلة المستنصرية للعلوم والتربية 414–17:399;2016.

[3] Mohammed NA, Ebrahiem SA. Study of Lung Cancer Hazard Due to Radiate Radon Gas for Two Factories in Industrial Region (Shaikh Omar) of Baghdad Governorate. Ibn AL-Haitham Journal For Pure and Applied Sciences 2020;33:27–33.

[4] Abbas SA, Salman SH, Ebrahiem SA, Tawfeek HM. Investigation of the nuclear structure of some ni and zn isotopes with Skyrme-Hartree-Fock interaction. Baghdad Science Journal 2022;19:914.

[5] Ebrahiem SA, Younis TA. Finding Most Stable Isobar for Nuclides with Mass Number (165-175) against Beta Decay. NeuroQuantology 2021;19:15.

[6] Mohammed NA, Ebrahiem SA. Assessment of radiation risk parameters for natural radon in three Iraqi institutions for February. AIP Conf Proc, vol. 2307, AIP Publishing; 2020.

[7] Salim DA, Ebrahiem SA. Study of nuclear properties for the carbon (C) and oxygen (O) isotopes: Deformation parameters and root mean square radii. AIP Conf Proc, vol. 2398, AIP Publishing; 2022.

[8] Hassan IM, Ebrahiem SA, Al-Khafaji RSA. Calculated the quadrupole electrical transmission| M (E2)| 2 Wu↓ for even-even nuclides of strontium (78-100Sr and 66-76Ge). AIP Conf Proc, vol. 2437, AIP Publishing; 2022.

[9] Hammoodi FG, Shuihab AA, Ebrahiem SA. Studying The Topographic and Morphology Structure of CdO: In Thin Films. J Phys Conf Ser, vol. 1963, IOP Publishing; 2021, p. 012121.

[10] Ali TAA, Ebrahiem SA. Study of the cross-sections of neutron interaction with lithium isotopes according to the reaction of the reverse reaction. AIP Conf Proc, vol. 3018, AIP Publishing; 2023.

[11] Mohammed SJ, Aobaid AK, Ebrahiem SA. Calculation of total stopping power of the radioactive isotopes of carbon-14 and florine-18 used to treat cancer patients. AIP Conf Proc, vol. 3018, AIP Publishing; 2023.

Ebrahiem SA, Sarsam MN, [12] Youhana HM, Abd-Al-Hameed NT. Determining of Cross Sections for 16O (n, α) 13C reaction from Cross Sections of 13C (α, n) 16O for the ground state. Ibn AL-Haitham Journal For Pure and .Applied Science 2017;26:109–15

[13] Mohammed SJ, Aobaid AK, Ebrahiem SA. Calculation of protons stopping power in Yttrium-90 and Iodine-131 radioactive isotopes. AIP Conf Proc, vol. 3018, AIP Publishing; 2023.

Al-Sarray E, Noori SS, [14] Ebrahiem SA. Investigation of camel hair has a high ability to attenuate gamma rays. AIP Conf Proc, vol. 2398, .AIP Publishing; 2022

[15] Lalazissis GA, Raman S, Ring P. Article ID adnd.1998.0795, available online at Atomic Data and Nuclear Data Tables. vol. 71. 1999.

[16] Firestons RB, Shirley VS. Table of isotopes eighth edition, Newyork 1999.

[17] Youhana HM, Ebrahiem SA. Determining of Cross Sections for 22Na (n, Î±) 19F reaction from Cross Sections of 19F (Î±, n) 22Na reaction using the reciprocity theory for the ground state. Ibn AL-Haitham Journal For Pure and Applied Sciences 2009;22.

[18] Salim DA, Ebrahiem SA. Study of transition strength for two isotopes carbon and oxygen. AIP Conf Proc, vol. 2437, AIP Publishing; 2022.

[19] Angeli I, Marinova KP. Table of experimental nuclear ground state charge radii: An update. At Data Nucl Data Tables 2013;99:69–95.

[20] Raman S, Nestor Jr CW, Tikkanen P. Transition probability from the ground to the first-excited 2+ state of even–even nuclides. At Data Nucl Data Tables 2001;78:1–128.